

A High-Performance 75 W Direct Ammonia Fuel Cells Stack

Teng Wang, Yun Zhao*, Brian P. Setzler, Reza Abbasi, Shimshon Gottesfeld and Yushan Yan

Department of Chemical and Biomolecular Engineering, Centre for Catalytic Science and Technology
University of Delaware, Newark, DE 19716

ABSTRACT

Ammonia can be directly used as fuel to generate electric energy in a low-temperature direct ammonia fuel cell (DAFC), making the DAFC an attractive option for zero-emission transportation. However, with a high-performance and durable DAFC still to be demonstrated, and with the remaining need to identify a suitable first market, the introduction of this technology has been delayed so far. Here, we report a high-performance DAFC stack enabled by a hydrophobic spinel cathode, which achieves the best combination of performance and durability reported to date. Peak power density of 410 mW cm^{-2} and continuous operation for 80 hours at 300 mA cm^{-2} were achieved for the first time in 5 cm^2 DAFCs, and then successfully scaled up to 50 cm^2 . Five such cells were assembled into a 75 W DAFC stack using graphite bipolar plates, demonstrating stack performance at the level expected from the single cell tests. The best combination of performance and durability for the single cell and, particularly, the demonstration of the world's first DAFC bipolar stack, constitute significant milestones in the development of DAFC technology. We also performed an in-depth techno-economic analysis of a 2 kW, 10 kWh DAFC system serving as power source for drones. Based on the DAFC performance demonstrated by us to date, such system can be a competitive power source over hydrogen fuel cells and Li-ion batteries.

*Corresponding authors: e-mail: yzhao@udel.edu

Decarbonization of various sectors of the economy has become a major target, particularly so in the case of the transportation sector¹⁻³. At the same time, ammonia has been gaining recognition as alternative fuel of significant potential for decarbonization of that sector. This recognition is based on the fuel's high energy density, large-scale global production, extensive existing infrastructure, and low cost per unit energy⁴⁻¹¹. The recent attention to ammonia/air fuel cell power sources, is explained by this rising interest in ammonia as a non-carbon, alternative fuel for transportation¹²⁻²⁶. Low-temperature direct ammonia fuel cell (DAFC) has two important features of low temperature operation and direct use of the fuel stored on board as the anode feed stream. The importance of these two characteristics has been demonstrated by the successful commercialization of proton exchange membrane fuel cells (PEMFCs) as power sources for vehicles. The power system simplicity and the absence of high temperature fuel processing upstream the stack, are common to fuel cells with the direct H₂ and NH₃.

The optimum temperature for the operation of the DAFCs is ~100 °C -- a compromise between (i) the need of higher cell temperature for enhancing the rate of the sluggish ammonia oxidation reaction (AOR) and, (ii) the upper limit of cell temperature defined by the demands of thermal stability for all cell components. As shown by us before^{6,12,13,16,27,28}, the operation of the DAFC near 100 °C addresses to significant degree the power density demand, while leaving the door open for the use of ionic membranes -- the electrolyte of choice for low temperature fuel cells over the last 60 years. Indeed, the significant advances reported in recent years in performance and longevity of the DAFCs, were enabled by the progress in the development of hydroxide exchange membranes (HEMs) of high conductivity, and improved chemical and mechanical stability²⁹. Such HEMs are a critical requirement for the development of polymer electrolyte DAFCs, as the

proton conducting ionomers used for hydrogen fuel cells are deactivated by even ppm levels of ammonia, converting the protons in the ionomer to ammonium cations³⁰.

With the quality of HEMs improving significantly, more recent DAFC R&D efforts have targeted electrocatalysts of higher activity, and cell structures and operation conditions that secure an optimized distribution of an aqueous component across the cell thickness dimension. The anode catalysts identified to date as most active in the AOR at cell temperature below 120 °C, are based on Pt and Ir, in the form of either a binary alloy or the mixtures of Pt and Ir components. The limited catalytic activity of even these most active catalysts and the limited useful range of anode overpotentials available for the AOR at Pt and/or Ir catalysts, explain the requirement of cell operation at ~100 °C as the condition for reaching high peak power densities³². The choice of a cathode catalyst for the DAFC has been directed by (i) the desire to avoid use of any platinum group metal (PGM) beyond the high loadings of such catalysts required to date in anode and, (ii) a minimal effect of any contact with ammonia on the catalyst oxygen reduction reaction (ORR) activity. The latter directive stems from the recognition that some crossover of aqueous ammonia into the cathode is existing in DAFCs used to date. Coupling with ammonia crossover, our previous work further shows that the cathode of DAFCs is subjected to severe flooding due to high water concentration gradient from anode to cathode and high water permeability of HEMs²⁷. As such, an ideal cathode is a cathode with an ORR catalyst that is highly tolerant to ammonia and highly resistant to flooding, allowing for the best combination of cell performance and durability.

Because a single cell cannot produce enough power output for transportation application, there is a crucial need to develop a DAFC stack consisting of a number of individual cells that can be ultimately built into a system. In addition to high-performance single DAFC requiring advanced materials and optimized operating conditions, the rational design for DAFC stacks is also an

important factor to attain a high-performance DAFC stack. The bipolar plate design is critical because it is the key component in bipolar fuel cell stacks³³⁻³⁶. As for the bipolar plate's material selection, the most popular materials are metals and graphite composites^{37,38}. Graphite offers low interfacial contact resistance and high resistance to corrosion by ammonia and potassium hydroxide. Still, some commonly used resins in composite graphite plates have insufficient chemical resistance, including vinyl ester and acrylic resins. A commercially available graphite-polypropylene composite bipolar plate was chosen to provide the necessary chemical resistance. Shunt current is also a particularly acute concern in DAFC stacks with graphite bipolar plates because strong base electrolyte, which is usually added into ammonia fuel for acquiring high cell performance, circulates through the anode side and leads to potential corrosion of graphite bipolar plates. Thus, minimizing the harmful effects of shunt current is essential for the designers of DAFC stacks. Also, compression load plays an important role in the performance of the stacks in a complex manner³⁹⁻⁴¹.

Ultimately, a system including all necessary components will be needed to operate a DAFC stack to fulfill the practical application. From a commercialization perspective, the promising first-market which is the best fit for DAFCs is drones (unmanned aerial vehicles), particularly for agricultural use. In this industry, drones are commonly equipped for aerial photography, hyperspectral surveying, or nutrient/pesticide delivery. The majority of these businesses' emphasis is on taking heavy loads beyond the visual line of sight due to the large land areas they need to cover. Battery-powered drones are popular for the current drone market, but one of the biggest obstacles is their short flight time under 40 minutes⁴². Hydrogen-powered drones are beginning to enter the plug-and-play drone market⁴³. However, the main challenge of using hydrogen-powered drones is hydrogen availability and transportation. We posit that it would remain highly

competitive if a DAFC device can provide at least two hours of autonomy and be rated for at least 2 kW of power.

In the present work, we report a high-performance DAFC stack based on hydrophobic spinel cathodes and optimal stack designs. Firstly, ORR activities of three spinel catalysts (Co_2MnO_4 , Co_2FeO_4 , and Co_3O_4) in the presence of ammonia are examined in DAFCs for the first time. Co_2MnO_4 provides superior performance in both ex-situ rotating disk electrode (RDE) experiments and in-situ DAFC tests. A hydrophobic cathode containing a hydrophobic agent (PTFE) in the catalyst layer is carefully designed to improve DAFCs' performance and durability significantly. With optimized conditions, a power density of 410 mW cm^{-2} is achieved, exhibiting comparable cell performance with the state-of-the-art of DAFC, and the best durability for DAFCs to date is also realized, showing a continuous voltage output for 80 hours at 300 mA cm^{-2} with an average decay rate of 1.6 mV/h . Secondly, a 75 W DAFC stack comprising five individual 50 cm^2 cells, designed by considering the shunt current issue based on graphite bipolar plates, is demonstrated to operate at $90 \text{ }^\circ\text{C}$. Finally, a 2 kW, 10 kWh DAFC-based system is analyzed to project the system efficiency and energy density and is compared to hydrogen and battery alternatives. This work represents pioneering results and further sheds new light on DAFCs technology development for practical applications.

Evaluation of Spinel ORR catalysts for use in the DAFC cathode

A variety of transition metal spinels exhibiting significant ORR catalytic activity have been discussed in the literature⁴⁴, in which the ORR activity of spinel catalysts exhibits a volcano trend versus the occupancy of e_g orbitals in the coordination structure of octahedral sites. For the case of a DAFC cathode, the selection of a specific catalyst should be based on the ORR activity measured at the catalyst/aqueous base interface and the degree of interference by ammonia.

Ammonia could affect the rate of the ORR at a cathode catalyst surface by adsorption of NH_3 and/or surface intermediates formed by AOR at catalyst sites active due to the coordination effect, which may also varies with different occupancy of e_g orbitals. Ammonia could also affect the performance of the cathode catalyst by generating a faradaic, ammonia oxidation current at the cathode catalyst, thereby reducing the net cathode current at some given cathode overpotential. Herein, the ORR activities of three Co_2MO_4 catalysts ($M = \text{Mn, Fe, Co}$) with different e_g occupancy of the metallic cation in octahedral sites were evaluated for their activity in the presence of ammonia. Figure 1 presents the j_{ORR} vs. potential (vs. RHE) dependence measured for the three spinel catalysts using a RDE in the presence and absence of ammonia. The effect of ammonia on cathode polarization is seen to be small in all cases, meaning that these spinel catalysts are not deactivated substantially in contact with ammonia nor do they generate a significant AOR current in the relevant cathode potential range. Co_2MnO_4 offers the best ORR activity in the presence of ammonia, as it does in an ammonia-free electrolyte. The measured mass activity for Co_2MnO_4 at 0.85 V vs. RHE at 25 °C is 119 mA mg^{-1} , quite higher than that of Co_2FeO_4 (40 mA mg^{-1}) and Co_3O_4 (35 mA mg^{-1}). It should be noted that the ORR activity loss of Co_2MnO_4 is much lower than that of Pt catalyst by comparing the shift of their half-wave potential after ammonia is added. The half-wave potential of Co_2MnO_4 slightly shifts by 20 mV (from 0.86 to 0.84 V vs RHE) while Pt catalyst exhibits a shift of half-wave potential by 50 mV (from 0.9 to 0.85 V vs RHE) in previous work⁶.

To examine their performance as catalysts in DAFCs, Co_2FeO_4 , Co_2MnO_4 , and Co_3O_4 catalyst were sprayed on the cathode side of HEM to create catalyst coated membrane (CCM) with hydroxide exchange ionomer (HEI) as described in previous reports^{6,27}. DAFCs with the above-mentioned cathodes and PtIr/C anodes, were assembled and tested by feeding the anode with a 7

M NH₃ in 1.25 M KOH solution. Figure 2 shows that the best cell performance was obtained for the DAFC with the Co₂MnO₄ cathode catalyst, agreeing well with the RDE results. A peak power density of 235 mW cm⁻² was achieved with the Co₂MnO₄ cathode catalyst when operating at temperature of 110 °C. Additionally, a continuous DAFC operation for 63 hours is observed at 300 mA cm⁻², operating at 100 °C. Although there is still degradation and voltage fluctuation issues, this DAFC durability has been better than the DAFC that has Acta 4020 cathode, which shows a dramatic degradation caused by its specific micropores structure (most active sites are located inside of micropores and thus are easier to be blocked by water) in previous report^{27,45}. Based on these results, the Co₂MnO₄ catalyst is selected for further investigation.

Facilitating oxygen transport through the cathode by addition of PTFE

The performance of a cathode in a polymer electrolyte fuel cell is determined jointly by the kinetics of the ORR and the oxygen transport resistance of the cathode catalyst layer (CL), where the latter could have a significant effect on the performance at higher current densities²⁷. Previous experimental results suggested that uptake of liquid water by a more hydrophilic cathode CL, can result in oxygen transport limitations^{46,47}. With an aqueous solution of ammonia fed to the anode of the DAFC, significant cathode flooding can result from water crossover driven by a steep water concentration gradient between anode and cathode and facilitated by the high water permeability of HEMs. Supplementary Fig. 1 shows that the rate of water exiting the cathode exhaust when the anode feed is aqueous ammonia, is significantly higher than that measured when the anode feed is a hydrogen/water vapor mixture. This indicates a significant rate of liquid water crossover from anode to cathode in DAFC, with most of this water crossing through the cathode catalyst layer before exiting via the cathode exhaust. To reduce this flooding tendency, we used a more hydrophobic cathode CL, where PTFE was incorporated into the catalysts layer coated on a gas

diffusion layer. As seen in Figure 3a, the contact angle of water for the surface of the PTFE-containing gas diffusion electrode (GDE) was 140° compared with 40° for a CCM using only ionomer as the bonding agent in the CL. Hence, the hydrophobic GDE should present better resistance to flooding by liquid water, and thereby mitigate oxygen transport in the catalyst layer.

The improved oxygen transport rate expected for the hydrophobic GDE, is confirmed by an ORR limiting current test based on a half-MEA design (Supplementary Fig. 2). With neat oxygen at 100% RH and 25°C , the CCM and GDE show a comparable ORR activity (Supplementary Fig. 3). However, when a cathode feed with a small fraction of oxygen ($0.2\% \text{O}_2$ in N_2) is used and the operating temperature is elevated to 70°C , the cell with PTFE added to the cathode CL exhibits clearly a higher limiting current, suggesting that the added PTFE can better secure high oxygen transport rate under conditions of significant water crossover.

Performance and durability of a single cell with a cathode CL containing PTFE

A performance comparison of two DAFCs employing GDE and CCM-based cathodes is shown in Figure 4a. Following area-specific resistance (ASR) correction ($85 \text{ m}\Omega \text{ cm}^{-2}$ and $69 \text{ m}\Omega \text{ cm}^{-2}$ for DAFCs with GDE-based and CCM-based cathode, respectively), the DAFC with the GDE-based cathode (PTFE added) exhibits higher performance than the DAFC with the CCM-based cathode (no PTFE added), confirming the merit of adding PTFE to the cathode CL. We also studied the effect of varying the Co_2MnO_4 loading in the cathode on DAFC performance. As seen in Supplementary Fig. 4, the DAFC performance increases with Co_2MnO_4 loading in the cathode between 0.2 mg cm^{-2} to 1.2 mg cm^{-2} , and the Co_2MnO_4 loading of 1.2 mg cm^{-2} provides the best performance showing an improved performance in the low current density regions.

Because PTFE is a non-hydroxide conductive material and can not act as an ionomer to facilitate hydroxide ion transport in the catalysts layer, the high ASR value in the GDE configuration is

observed. Ion transport's function in the catalyst layer of the GDE configuration is completely dependent on penetrated KOH across the membrane from the anode feedstock. Consequently, we increase KOH concentration from 1.25 M to 3 M in anode fuel to reduce the ASR of the cell. As is shown in Figure 4b, rising KOH concentration can further reduce the ASR of the cell ($85 \text{ m}\Omega \text{ cm}^{-2}$ for 1.25 M KOH vs. $60 \text{ m}\Omega \text{ cm}^{-2}$ for 3 M KOH). This leads to a significant increase in cell performance, achieving a peak power density of 410 mW cm^{-2} that is comparable to the performance of the state-of-the-art DAFC (420 mW cm^{-2})¹².

Most importantly, in addition to the top-performing DAFC enabled by the hydrophobic GDE configuration, the use of the hydrophobic GDE significantly can improve the DAFC stability. Figure 4c shows the voltage-time plot for a DAFC with a PTFE-containing cathode CL, demonstrating continuous operation for 80 hours at 300 mA cm^{-2} with an average voltage loss rate of 1.6 mV/hour . Both the rate of voltage loss and the accompanying increase in ASR (from $60 \text{ m}\Omega \text{ cm}^2$ to $90 \text{ m}\Omega \text{ cm}^2$) are much smaller than those recorded for DAFCs with a more hydrophilic cathode CLs and/or with other types of cathode catalysts²⁷. It should be noted that a highly stable voltage output is obtained in comparison to a fluctuating voltage output for the CCM based DAFC. Recognizing that the overall performance of the DAFC is largely dominated by anode voltage losses, these results highlight the significance of the cathode catalyst and the prevention of cathode flooding in the determination of the DAFC's performance and stability.

The reason for the degradation rate of 1.6 mV/h , accompanied by an increase in ASR over time, is likely gradual chemical degradation of the HEM to decrease its ion exchange capacity (IEC) during continuous operation, especially in a harsh condition (3 M KOH and $100 \text{ }^\circ\text{C}$)^{29,48,49}. As shown in Supplementary Fig. 5, a remarkable reduction in ammonia crossover was observed following the 80 h test: 149 mA cm^{-2} at the end vs. 346 mA cm^{-2} at the start. Such drop in ammonia

crossover is likely the consequence of HEM degradation. Another possible reason is AOR catalysts deactivation caused by the formation of strongly chemisorbed ammonia oxidation intermediates during the stability test^{32,50-52}.

Building and testing a 5-cell DAFC stack of 50 cm² cell area

The performance of the 50 cm² MEA used in the DAFC stack described below, was examined first in a single cell which was assembled using elements of the stack hardware acquired. This hardware imposed an upper limit of 90 °C on the cell temperature during testing, defined by the softening temperature of polypropylene which is chosen as sealant for the graphite plates to ensure hardware immunity to ammonia. The polarization curve recorded for this single cell is shown in Figure 5c, revealing a peak power density of 300 mW cm⁻². This peak power is lower than that of the 5 cm² single cell (Figure 4) due to the lower operating temperature (90 °C vs. 110 °C) and the higher ASR (110 mΩ cm² vs. 60 mΩ cm²). The higher ASR was caused, in part, by the higher contact resistance (87 mΩ cm², Supplementary Fig. 6), both in the bipolar plates and current collectors. Each bipolar plate is made of two half plates to provide cooling channels, which adds an interface. Additionally, the 50 cm² single cell graphite hardware was compressed less tightly than our 5 cm² hardware, resulting in a higher contact resistance at the graphite plate/current collector interface. In a stack, the current collector related resistance is amortized across many cells and, consequently, has a lower impact.

We next looked into optimized stack parameters, including the number of cells to be used and the optimal clamping load. The number of cells selected was determined by the shunt currents calculated for the configuration of our stack hardware which was based on a common inlet manifold supplying the anode feed to each of the cells. When a fuel feed consisting of ammonia mixed with strong base electrolyte (KOH), enters through such inlet manifold, distributes to the

individual cells, and recombines and leaves through an exit manifold, the large potential difference between the first and last bipolar plate can cause carbon corrosion. To some extent, the potential difference between the plates is mitigated by potential gradients in the electrolyte caused by shunt currents flowing between cells. Supplementary Note 1 provides a calculation of the shunt currents and plate surface potentials based on an equivalent circuit (Supplementary Fig. 7) representing the anode manifold of a five-cell stack. At single cell voltage of 0.5 V, the highest plate surface potential in a 5-cell stack of manifold dimensions employed, is calculated about 1.15 V vs RHE, which avoids severe carbon corrosion. A stack of larger cells number could be built by using bipolar plates with an insulating frame and conductive active area, so that the manifold surfaces are not conductive. The optimal clamping load for the stack was evaluated before DAFC stack assembly, by examining the effect of a range of torques (1.36 N.m, 2.03 N.m, 2.71 N.m, and 3.34 N.m) on the quality of the interfacial contact (Supplementary Fig. 8). Pressure paper tests (Supplementary Fig. 9) showed that the quality of the contact increased with the torque all the way up to 3.34 N.m and we consequently used a torque of 3.34 N.m for clamping the stack.

The assembled 5-cell DAFC stack which generated 75W of electric power, is illustrated in Figure 5a and its polarization characteristic is presented in Figure 5b. Remarkably, the average peak power density of 300 mW cm^{-2} for the cells in the stack is identical to the power density of the single cell with the same surface area. The PTFE containing cathode CL and in-house fabricated spinel catalyst were used in the five MEAs in the stack. The variation of the DAFC stack voltage over time operating at $90 \text{ }^\circ\text{C}$ and constant current of 15 A, is shown in Figure 5d. This stack was operated first for 3.5 h before shutting it down for the night, and the voltage degradation is seen to slightly recover on stack restart on the next day. The beneficial effect of

open-circuit conditions on recovery of the DAFC anode performance has been explained by reductive desorption of strongly bonded AOR intermediates at the PtIr catalyst⁵⁰.

Projections in 2 kW, 10 kWh DAFC-based drone power system

Based on the DAFC stack prototype developed, we consider here the possible use of a DAFC-based power system using liquid ammonia as the fuel on board for powering a drone. We have made projections of the competitiveness of a drone power source based on a DAFC vs. a PEMFC fueled by hydrogen and vs. battery alternatives. A DAFC system described in Figure 6a, includes a stack, a fuel tank, liquid ammonia fuel, and the balance of plant (BOP) which includes a compressor-expander module for the airflow, membrane humidifier, anode fuel mixer, recycle pump, condenser, and an ammonia scrubber. Projections of the mass and volume for a 2 kW, 10 kWh drone power system are shown in Supplementary Table 1. Using the measured polarization curve for the 75 W stack, the calculated system efficiency is given as a function of ammonia crossover in Figure 6b, indicating that the loss of ammonia by crossover measured in such DAFCs has a strong impact on system efficiency. For example, with an ammonia crossover rate of 346 mA cm⁻² measured for one single DAFC tested near 100 °C (Supplementary Fig. 5), the calculated system efficiency at cell current of 300 mA cm⁻² generated at cell voltage of 0.47 V, is 17 %. At the same cell current and voltage, system efficiency will be improved to 35 % or 33 % if ammonia crossover could be reduced to 0 mA cm⁻² or 25 mA cm⁻², respectively. As the system efficiency have been calculated based on the polarization characteristic of the 75 W stack (Figure 5b), and the efficiency can also be increased by operation with the same catalysts at somewhat higher cell temperature or, ultimately, with advanced MEAs of higher intrinsic performance. The most important barrier, however, to higher DAFC efficiency, is loss of fuel by ammonia crossover that could be most effectively treated using a selective barrier for blocking ammonia and

simultaneously maintaining high OH⁻ ion conductivity. For instance, system efficiency of 42 % could be reached with the ultimate target - 0.58 V at 300 mA cm⁻² and ammonia crossover of 25 mA cm⁻².

Because energy density is the key metric for drones, specific energy densities (mass and volume) of 2 kW, 10 kWh DAFC-based drone power systems were estimated by calculating the contributions of the stack, the full fuel tank, and BOP to the system mass and volume (Supplementary Note 2). As seen in Figure 6c, with operation point of the DAFC stack of 0.47 V per cell at 300 mA cm⁻² and ammonia crossover of 346 mA cm⁻², the gravimetric and volumetric energy densities are 0.4 kWh kg⁻¹ and 0.3 kWh L⁻¹, respectively. With an ultimate target of 0.58 V at 300 mA cm⁻² and ammonia crossover limited to 25 mA cm⁻², the gravimetric and volumetric energy densities could be improved to 0.65 kWh kg⁻¹ and 0.5 kWh L⁻¹, respectively. In comparison, the hydrogen fueled system has energy densities of 0.52 kWh kg⁻¹ and 0.22 kWh L⁻¹, and the battery possesses energy densities of 0.2 kWh kg⁻¹ and 0.4 kWh L⁻¹. The results show that the DAFC-based power system for drones would be highly competitive by following a significant reduction of the ammonia crossover and further enhancement of the cell power output. Further work along these lines has been pursued.

Conclusions

In summary, we report here significant advancements in polymer electrolyte DAFC technology at the cell and the stack levels. The cell performance and durability have both been well advanced by use of a spinel ORR catalyst, Co₂MnO₄, which was synthesized in-house and examined in DAFC cathode for the first time. This catalyst offered the best performance in both ex-situ RDE measurements and DAFC tests. A hydrophobic DAFC cathode employing the Co₂MnO₄ catalyst

enabled a high peak power density of 410 mW cm^{-2} , and importantly, the best DAFC durability reported to date, an 80 hours run at 300 mA cm^{-2} . A first DAFC stack of 75 W was successfully assembled using the hydrophobic Co_2MnO_4 cathodes and PtIr/C anode catalysts. The 5 cell, 50 cm^2 stack was built of graphite hardware and exhibited average cell performance practically identical to that of a single 50 cm^2 cell. The shunt currents estimated from the dimensions of the manifold in the stack, defined the number of cells allowed in the (unmodified) stack. Finally, a 2 kW, 10 kWh DAFC-based power system for drones has been evaluated vs. a hydrogen fueled FC system and a Li-ion battery. The work presented in this manuscript demonstrates the state-of-the-art in DAFC technology, and provides critical insights towards the further development of high-performance DAFC power sources that could be used as energy-efficient, carbon-neutral power systems for transportation.

Acknowledgments

The information, data, or work presented herein was funded in part by the Advanced Research Projects Agency-Energy (ARPA-E), U.S. Department of Energy, under Award Number DE-AR0000805. The views and opinions of authors expressed herein do not necessarily state or reflect those of the United States Government or any agency thereof.

Competing interests

The PiperION membranes and ionomers were provided for free by Versogen, a company co-founded by some of the coauthors of this article.

Methods

Synthesis of spinel catalysts

Co_2MO_4 (M = Mn, Fe, Co) was synthesized as follows⁴⁴. $\text{Co}(\text{OAc})_2 \cdot 4\text{H}_2\text{O}$ (127.5 mg, Sigma-Aldrich) was firstly dissolved in 24 mL ethanol, and then 60 mg Vulcan XC-72R carbon was added into the solution. The mixture was sonicated for 10 min and following by adding dropwise the mixture of 0.44 mL ammonia (28 wt%) and 20 mL ethanol. After the suspension was sonicated for 10 min, the solution of $\text{Mn}(\text{OAc})_2 \cdot 4\text{H}_2\text{O}$ (62.5 mg, Acros), $\text{Fe}(\text{NO}_3)_3 \cdot 9\text{H}_2\text{O}$ (103 mg, Sigma-Aldrich), or $\text{Co}(\text{OAc})_2 \cdot 4\text{H}_2\text{O}$ (63.8 mg, Sigma-Aldrich) dissolved in 1.5 mL water was added. The final suspension was heated at 60 °C for 12 h under reflux and then transferred to Teflon autoclave for the hydrothermal reaction at 150 °C for 3 h. The Co_2MO_4 product was collected by centrifugation and thoroughly washed with water and ethanol, then dried under vacuum.

Ex-situ RDE experiments

The ORR catalysts sample (1 mg) was ultrasonically dispersed in 1 mL mixed solvent of ethanol and water (1:1 v/v), and then 10 μL of Nafion solution (5 wt% in ethanol) was added to the suspension. The suspension was dropped onto a rotating disk electrode (5.0 mm in diameter) with a glassy carbon substrate and dried for 2 h at room temperature to fabricate the electrodes. The catalyst loading was 0.028 mg cm^{-2} . The electrochemical measurement on RDE was performed in a standard three-electrode system controlled by Biologic VMP-2 potentiostat. A clean graphite rod is used as the counter electrode, and a saturated Ag/AgCl electrode is used as the reference electrode.

Membrane-electrode-assemblies (MEAs) preparation

Anode was prepared by coating PtIr/C catalysts on carbon cloth with the catalyst loading of $2 \text{ mg}_{\text{PGM}} \text{ cm}^{-2}$. Utilizing isopropanol as the solvent and PiperION TP-100 ionomer (PtIr/C: PiperIon=9:1), the anode PtIr/C catalyst ink was ultra-sonicated in an ice-water bath for 1 h to form the uniform dispersion. The CCM-based cathode was prepared by spraying spinel catalysts with a weight ratio of 8:2 to PiperION TP-100 ionomer. The loading of spinel catalysts was 0.8 mg cm^{-2} . The GDE-based hydrophobic cathode was prepared by scrubbing CoMn_2O_4 catalysts with a weight ratio of 6.5:3.5 to PTFE binder. The loading was determined to 0.2, 0.8 and 1.2 mg cm^{-2} , respectively.

Single-cell and stack evaluation test

The default test conditions for a single-cell with an active area of 5 cm^2 or 50 cm^2 were anode fuel: 5 ml min^{-1} at 2 bar_g for the polarization curves test and 2 ml min^{-1} at 2 bar_g for the durability test; cathode fuel: $500 \text{ ml min}^{-1} \text{ O}_2$ at 100 % RH at 2 bar_g ; cell temperature: $110 \text{ }^\circ\text{C}$ for the polarization curves test and $100 \text{ }^\circ\text{C}$ for the durability test. The default test conditions for a 5-cell stack were anode fuel: 25 ml min^{-1} at 2 bar_g for the polarization curve test and 15 ml min^{-1} at 2 bar_g for the durability test; cathode fuel: $2500 \text{ ml min}^{-1} \text{ O}_2$ at 100 % RH at 3 bar_g for the polarization curve test and $1500 \text{ ml min}^{-1} \text{ O}_2$ at 100 % RH at 3 bar_g for the durability test; cell temperature: $90 \text{ }^\circ\text{C}$.

Data Availability

The data that support the plots within this paper and other findings of this study are available from the corresponding author upon reasonable request.

References

- 1 de Blas, I., Mediavilla, M., Capellan-Perez, I. & Duce, C. The limits of transport decarbonization under the current growth paradigm. *Energy Strateg Rev* **32**, doi:10.1016/j.esr.2020.100543 (2020).
- 2 Lefevre, J. *et al.* A pathway design framework for sectoral deep decarbonization: the case of passenger transportation. *Clim Policy* **21**, 93-106, doi:10.1080/14693062.2020.1804817 (2021).
- 3 Tayarani, M., Poorfakhraei, A., Nadafianshahamabadi, R. & Rowangould, G. Can regional transportation and land-use planning achieve deep reductions in GHG emissions from vehicles? *Transport Res D-Tr E* **63**, 222-235, doi:10.1016/j.trd.2018.05.010 (2018).
- 4 Valera-Medina, A., Xiao, H., Owen-Jones, M., David, W. I. F. & Bowen, P. J. Ammonia for power. *Progress in Energy and Combustion Science* **69**, 63-102, doi:10.1016/j.pecs.2018.07.001 (2018).
- 5 Kobayashi, H., Hayakawa, A., Somarathne, K. D. K. A. & Okafor, E. C. Science and technology of ammonia combustion. *P Combust Inst* **37**, 109-133, doi:10.1016/j.proci.2018.09.029 (2019).
- 6 Zhao, Y. *et al.* An Efficient Direct Ammonia Fuel Cell for Affordable Carbon-Neutral Transportation. *Joule* **3**, 2472-2484, doi:10.1016/j.joule.2019.07.005 (2019).
- 7 Lan, R. & Tao, S. Ammonia as a suitable fuel for fuel cells. *Frontiers in Energy Research* **2**, 1-4, doi:10.3389/fenrg.2014.00035 (2014).
- 8 Smith, C., Hill, A. K. & Torrente-Murciano, L. Current and future role of Haber-Bosch ammonia in a carbon-free energy landscape. *Energy & Environmental Science* **13**, 331-344, doi:10.1039/c9ee02873k (2020).
- 9 Hansson, J., Brynolf, S., Fridell, E. & Lehtveer, M. The Potential Role of Ammonia as Marine Fuel-Based on Energy Systems Modeling and Multi-Criteria Decision Analysis. *Sustainability-Basel* **12**, doi:10.3390/su12083265 (2020).
- 10 Cesaro, Z., Ives, M., Nayak-Luke, R., Mason, M. & Banares-Alcantara, R. Ammonia to power: Forecasting the levelized cost of electricity from green ammonia in large-scale power plants. *Appl Energy* **282**, doi:10.1016/j.apenergy.2020.116009 (2021).
- 11 MacFarlane, D. R. *et al.* A Roadmap to the Ammonia Economy. *Joule* **4**, 1186-1205, doi:10.1016/j.joule.2020.04.004 (2020).
- 12 Gottesfeld, S. The Direct Ammonia Fuel Cell and a Common Pattern of Electrocatalytic Processes. *Journal of the Electrochemical Society* **165**, J3405-J3412, doi:10.1149/2.0431815jes (2018).
- 13 Abbasi, R. *et al.* Low-temperature direct ammonia fuel cells: Recent developments and remaining challenges. *Current Opinion in Electrochemistry* **21**, 335-344, doi:10.1016/j.coelec.2020.03.021 (2020).
- 14 Guo, Y., Pan, Z. & An, L. Carbon-free sustainable energy technology: Direct ammonia fuel cells. *Journal of Power Sources* **476**, 228454, doi:10.1016/j.jpowsour.2020.228454 (2020).
- 15 Santamaria, A. D. & Mortazavi, M. Aqueous Ammonia Wetting of Gas-Diffusion Media for Electrochemical Cells. *Journal of The Electrochemical Society* **167**, 104507, doi:10.1149/1945-7111/ab995e (2020).
- 16 Achrai, B. *et al.* A Direct Ammonia Fuel Cell with a KOH-Free Anode Feed Generating 180 mW cm⁻² at 120 degrees C. *Journal of the Electrochemical Society* **167**, 134518, doi:10.1149/1945-7111/abdd1 (2020).
- 17 Jeerh, G., Zhang, M. F. & Tao, S. W. Recent progress in ammonia fuel cells and their potential applications. *Journal of Materials Chemistry A* **9**, 727-752, doi:10.1039/d0ta08810b (2021).
- 18 Lan, R. & Tao, S. W. Direct Ammonia Alkaline Anion-Exchange Membrane Fuel Cells. *Electrochem. Solid State Lett.* **13**, B83-B86, doi:10.1149/1.3428469 (2010).

- 19 Assumpcao, M. *et al.* Direct ammonia fuel cell performance using PtIr/C as anode electrocatalysts. *International Journal of Hydrogen Energy* **39**, 5148-5152, doi:10.1016/j.ijhydene.2014.01.053 (2014).
- 20 Assumpção, M. H. M. T. *et al.* Investigation of PdIr/C electrocatalysts as anode on the performance of direct ammonia fuel cell. *Journal of Power Sources* **268**, 129-136, doi:10.1016/j.jpowsour.2014.06.025 (2014).
- 21 Assumpção, M. H. M. T. *et al.* Oxidation of ammonia using PtRh/C electrocatalysts: Fuel cell and electrochemical evaluation. *Applied Catalysis B: Environmental* **174–175**, 136-144, doi:10.1016/j.apcatb.2015.02.021 (2015).
- 22 Suzuki, S., Muroyama, H., Matsui, T. & Eguchi, K. Fundamental studies on direct ammonia fuel cell employing anion exchange membrane. *Journal of Power Sources* **208**, 257-262, doi:10.1016/j.jpowsour.2012.02.043 (2012).
- 23 Lan, R. & Tao, S. W. Ammonia Carbonate Fuel Cells Based on a Mixed NH₄⁺/H⁺ Ion Conducting Electrolyte. *ECS Electrochem. Lett.* **2**, F37-F40, doi:10.1149/2.007305eel (2013).
- 24 Lee, K. R., Song, D., Park, S. B. & Han, J. I. A direct ammonium carbonate fuel cell with an anion exchange membrane. *Rsc Advances* **4**, 5638-5641, doi:10.1039/c3ra44057e (2014).
- 25 Okanishi, T., Katayama, Y., Muroyama, H., Matsui, T. & Eguchi, K. SnO₂-modified Pt electrocatalysts for ammonia-fueled anion exchange membrane fuel cells. *Electrochimica Acta* **173**, 364-369, doi:10.1016/j.electacta.2015.05.066 (2015).
- 26 Silva, J. C. M. *et al.* PtAu/C electrocatalysts as anodes for direct ammonia fuel cell. *Appl. Catal. A-Gen.* **490**, 133-138, doi:10.1016/j.apcata.2014.11.015 (2015).
- 27 Wang, T., Zhao, Y., Setzler, B. P. & Yan, Y. S. Improving Performance and Durability of Low Temperature Direct Ammonia Fuel Cells: Effect of Backpressure and Oxygen Reduction Catalysts. *Journal of the Electrochemical Society* **168**, doi:10.1149/1945-7111/abdcca (2021).
- 28 Li, Y. *et al.* High-Performance Ammonia Oxidation Catalysts for Anion-Exchange Membrane Direct Ammonia Fuel Cells. *Energy & Environmental Science*, doi:10.1039/D0EE03351K (2021).
- 29 Wang, J. H. *et al.* Poly(aryl piperidinium) membranes and ionomers for hydroxide exchange membrane fuel cells. *Nat Energy* **4**, 392-398, doi:10.1038/s41560-019-0372-8 (2019).
- 30 Uribe, F. A., Gottesfeld, S. & Zawodzinski, T. A. Effect of ammonia as potential fuel impurity on proton exchange membrane fuel cell performance. *Journal of the Electrochemical Society* **149**, A293-A296, doi:10.1149/1.1447221 (2002).
- 31 Uribe, F. A., Gottesfeld, S. & Zawodzinski, T. A. Effect of ammonia as potential fuel impurity on proton exchange membrane fuel cell performance. *J Electrochem Soc* **149**, A293-A296 (2002).
- 32 Herron, J. A., Ferrin, P. & Mavrikakis, M. Electrocatalytic Oxidation of Ammonia on Transition-Metal Surfaces: A First-Principles Study. *J. Phys. Chem. C* **119**, 14692-14701, doi:10.1021/jp512981f (2015).
- 33 Shaigan, N., Yuan, X. Z., Girard, F., Fatih, K. & Robertson, M. Standardized testing framework for quality control of fuel cell bipolar plates. *Journal of Power Sources* **482**, doi:10.1016/j.jpowsour.2020.228972 (2021).
- 34 Vargas, J. V. C., Ordonez, J. C. & Bejan, A. Constructal PEM fuel cell stack design. *Int J Heat Mass Tran* **48**, 4410-4427, doi:10.1016/j.ijheatmasstransfer.2005.05.009 (2005).
- 35 Barbir, F. in *Mini-Micro Fuel Cells*. (eds S. Kakaç, A. Pramuanjaroenkij, & L. Vasiliev) 27-46 (Springer Netherlands).
- 36 Włodarczyk, R. Properties of graphite-stainless steel composite in bipolar plates in simulated anode and cathode environments of PEM fuel cells. *Mater Sci-Poland* **32**, 487-497, doi:10.2478/s13536-014-0229-6 (2014).
- 37 Singh, R. S., Gautam, A. & Rai, V. Graphene-based bipolar plates for polymer electrolyte membrane fuel cells. *Front Mater Sci* **13**, 217-241, doi:10.1007/s11706-019-0465-0 (2019).

- 38 Song, Y. X. *et al.* Review on current research of materials, fabrication and application for bipolar plate in proton exchange membrane fuel cell. *International Journal of Hydrogen Energy* **45**, 29832-29847, doi:10.1016/j.ijhydene.2019.07.231 (2020).
- 39 Wu, C. W., Liu, B., Wei, M. Y. & Zhang, W. Mechanical Response of a Large Fuel Cell Stack to Impact: A Numerical Analysis. *Fuel Cells* **15**, 344-351, doi:10.1002/fuce.201400153 (2015).
- 40 Zhang, W. & Wu, C. W. Effect of Clamping Load on the Performance of Proton Exchange Membrane Fuel Cell Stack and Its Optimization Design: A Review of Modeling and Experimental Research. *J Fuel Cell Sci Tech* **11**, doi:10.1115/1.4026070 (2014).
- 41 Lee, S. Y., Lee, K. S. & Um, S. The structural variation of the gas diffusion layer and a performance evaluation of polymer electrolyte fuel cells as a function of clamping pressure. *J Mech Sci Technol* **22**, 565-574, doi:10.1007/s12206-007-1211-6 (2008).
- 42 Admirator. Top 10 Drones with the Longest Flight Times. (2020).
- 43 Arat, H. T. & Surer, M. G. Experimental investigation of fuel cell usage on an air Vehicle's hybrid propulsion system. *International Journal of Hydrogen Energy* **45**, 26370-26378, doi:10.1016/j.ijhydene.2019.09.242 (2020).
- 44 Wei, C. *et al.* Cations in Octahedral Sites: A Descriptor for Oxygen Electrocatalysis on Transition-Metal Spinels. *Advanced Materials* **29**, doi:10.1002/adma.201606800 (2017).
- 45 Wang, Y. C. *et al.* Constructing a Triple-Phase Interface in Micropores to Boost Performance of Fe/N/C Catalysts for Direct Methanol Fuel Cells. *Acs Energy Lett* **2**, 645-650, doi:10.1021/acseenergylett.7b00071 (2017).
- 46 Pasaogullari, U. & Wang, C. Y. Liquid water transport in gas diffusion layer of polymer electrolyte fuel cells. *Journal of the Electrochemical Society* **151**, A399-A406, doi:10.1149/1.1646148 (2004).
- 47 Das, P. K., Li, X. G. & Liu, Z. S. Analysis of liquid water transport in cathode catalyst layer of PEM fuel cells. *International Journal of Hydrogen Energy* **35**, 2403-2416, doi:10.1016/j.ijhydene.2009.12.160 (2010).
- 48 Dekel, D. R. *et al.* The critical relation between chemical stability of cations and water in anion exchange membrane fuel cells environment. *Journal of Power Sources* **375**, 351-360, doi:10.1016/j.jpowsour.2017.08.026 (2018).
- 49 Dekel, D. R. *et al.* Effect of Water on the Stability of Quaternary Ammonium Groups for Anion Exchange Membrane Fuel Cell Applications. *Chemistry of Materials* **29**, 4425-4431, doi:10.1021/acs.chemmater.7b00958 (2017).
- 50 Li, Z. F., Wang, Y. X. & Botte, G. G. Revisiting the electrochemical oxidation of ammonia on carbon-supported metal nanoparticle catalysts. *Electrochimica Acta* **228**, 351-360, doi:10.1016/j.electacta.2017.01.020 (2017).
- 51 Bunce, N. J. & Bejan, D. Mechanism of electrochemical oxidation of ammonia. *Electrochimica Acta* **56**, 8085-8093, doi:10.1016/j.electacta.2011.07.078 (2011).
- 52 Fu, G.-t. *et al.* L-Lysine mediated synthesis of platinum nanocuboids and their electrocatalytic activity towards ammonia oxidation. *Journal of Materials Chemistry A* **2**, 17883-17888, doi:10.1039/c4ta03601h (2014).

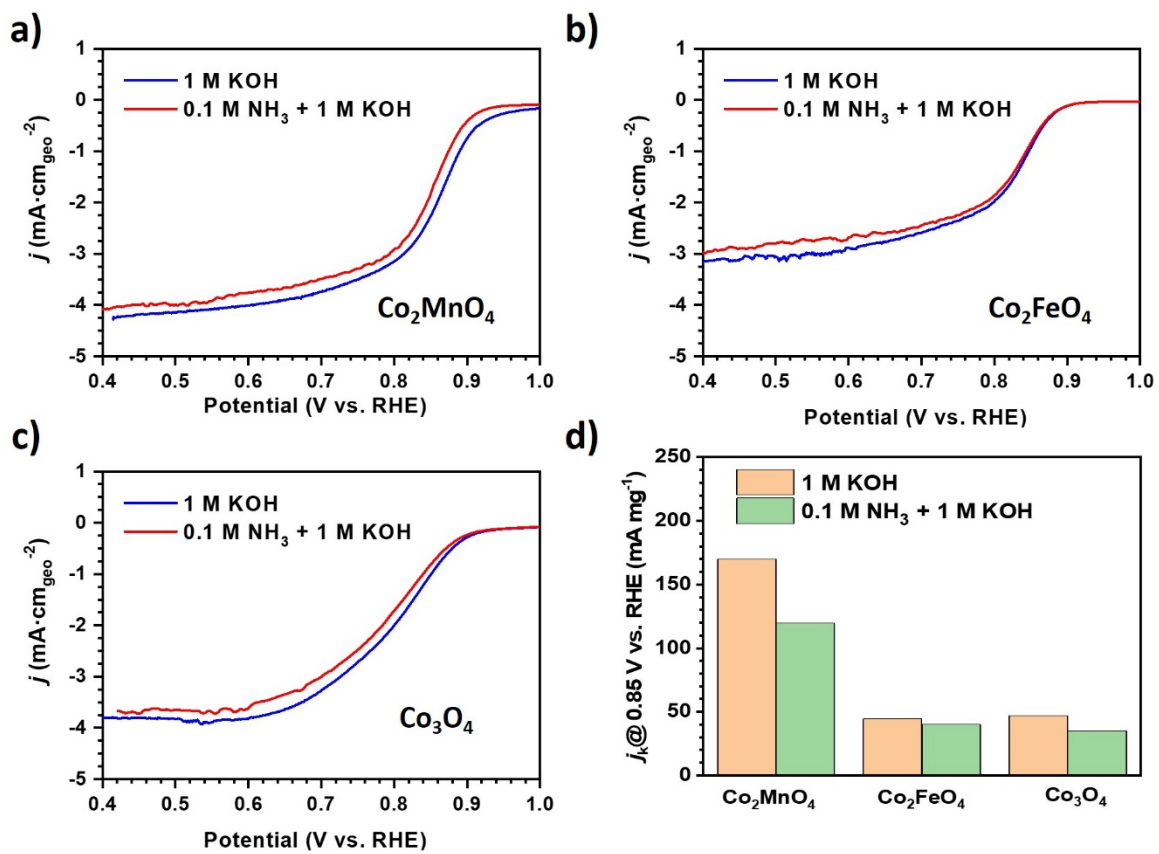


Fig. 1 | The ORR polarization curves in 1 M KOH and 0.1 M NH_3 - 1 M KOH solutions at room temperature. **a,** Co_2MnO_4 . **b,** Co_2FeO_4 . **c,** Co_3O_4 . **d,** The comparison of j_k at 0.85 V vs. RHE.

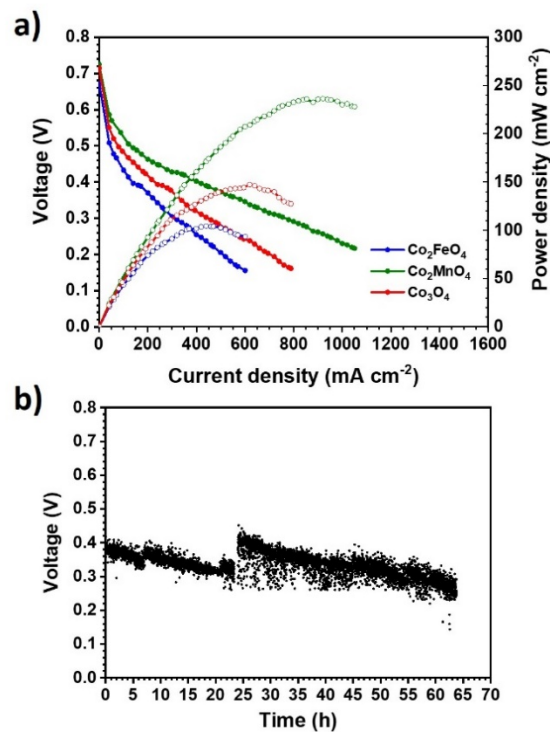


Fig. 2 | Performance and durability of DAFCs. **a**, Polarization and power density curves of DAFCs with different spinel catalysts based CCMs. Test conditions: cell temperature of $110\text{ }^{\circ}\text{C}$, 5 mL min^{-1} 7 M NH_3 in 1.25 M KOH at 2 bar_g , 0.5 L min^{-1} O_2 with a humidifier at $95\text{ }^{\circ}\text{C}$ and 2 bar_g . **b**, The durability test of the DAFC with different spinel catalysts based CCMs. Test conditions: at 300 mA cm^{-2} , cell temperature of $100\text{ }^{\circ}\text{C}$, 2 mL min^{-1} 7 M NH_3 in 1.25 M KOH at 2 bar_g , 0.5 L min^{-1} O_2 with a humidifier at $95\text{ }^{\circ}\text{C}$ and 2 bar_g . Anode: $2\text{ mg}_{\text{PGM}}\text{cm}^{-2}$ PtIr/C with PiperION PAP-TP-100 ionomer. HEM: PiperION membrane ($13\text{ }\mu\text{m}$ thickness, reinforced PAP-TP-85). Cathode: 0.8 mg spinel catalysts with $20\text{ wt}\%$ PiperION PAP-TP-100 ionomer.

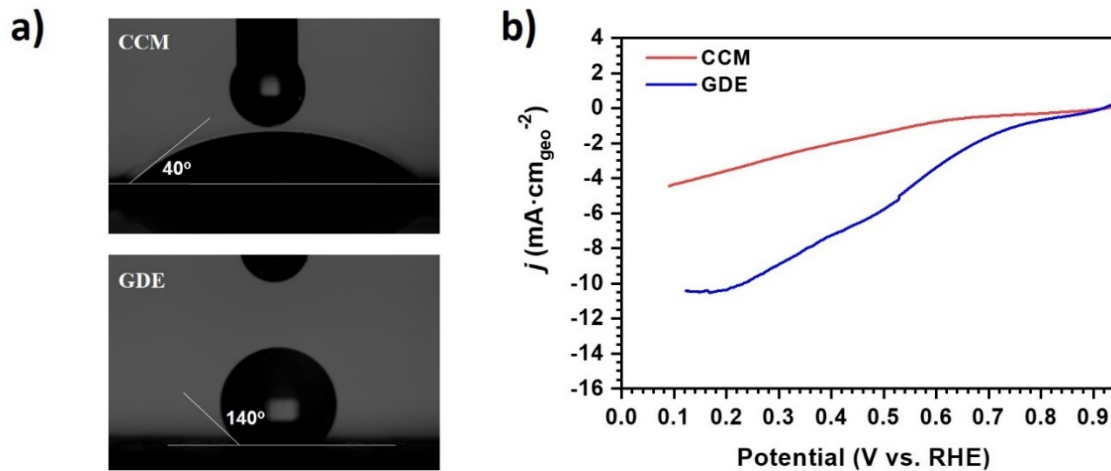


Fig. 3 | Characterization of hydrophobicity and the ORR limiting current of the cathodes with different configurations. a, Contact angle images of Co_2MnO_4 based CCM and GDE. **b,** ORR polarization curves of Co_2MnO_4 based CCM and GDE, respectively. Test conditions: 70 °C with a mixed flow (0.2 % O_2 in N_2) at 100 mL min^{-1} and 100 % RH.

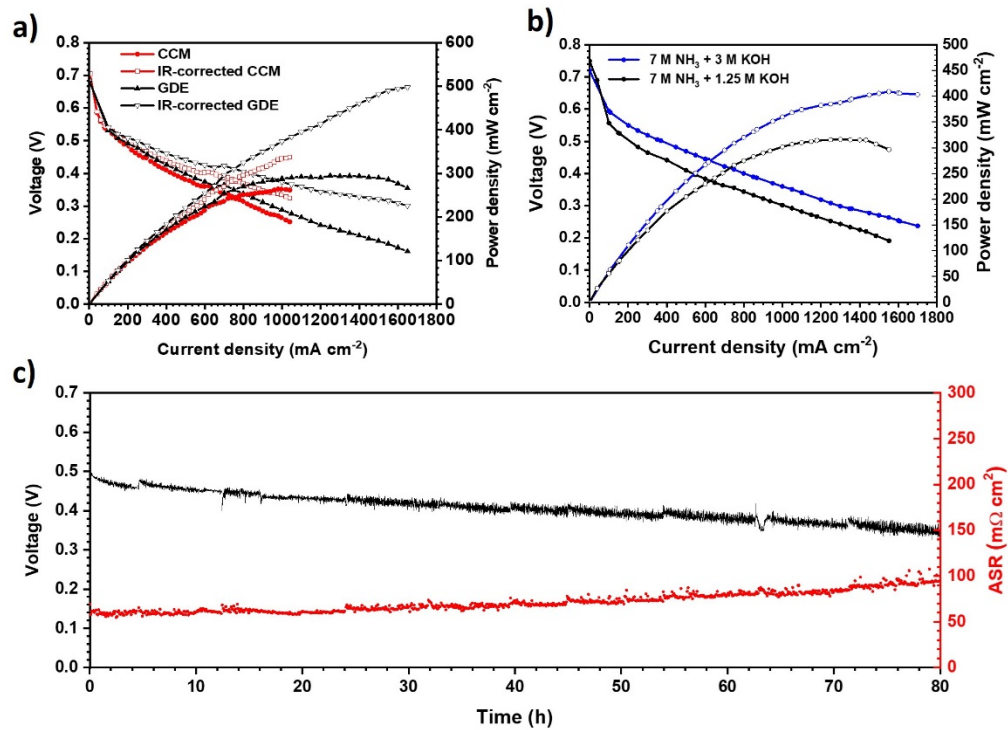


Fig. 4 | Performance and durability of DAFCs with Co_2MnO_4 catalysts. **a**, Polarization and power density curves of DAFCs with Co_2MnO_4 based CCM and GDE, respectively. **b**, Comparison of polarization curves of the DAFC with Co_2MnO_4 based GDE at different KOH concentrations in anode feed. Test conditions: cell temperature of $110\text{ }^\circ\text{C}$, 5 mL min^{-1} 7 M NH_3 in 1.25 M or 3 M KOH at 2 bar_g , 0.5 L min^{-1} O_2 with a humidifier at $95\text{ }^\circ\text{C}$ and 2 bar_g . **c**, The durability test of the DAFC with Co_2MnO_4 based GDE. Test conditions: at 300 mA cm^{-2} , cell temperature of $100\text{ }^\circ\text{C}$, 2 mL min^{-1} 7 M NH_3 in 3 M KOH at 2 bar_g , 0.5 L min^{-1} O_2 with a humidifier at $95\text{ }^\circ\text{C}$ and 2 bar_g . Anode: $2\text{ mg}_{\text{PGM}}\text{cm}^{-2}$ PtIr/C with PiperION PAP-TP-100 ionomer. HEM: PiperION membrane ($13\text{ }\mu\text{m}$ thickness, reinforced PAP-TP-85). Cathode: 1.2 mgcm^{-2} Co_2MnO_4 with $20\text{ wt}\%$ PiperION PAP-TP-100 ionomer.

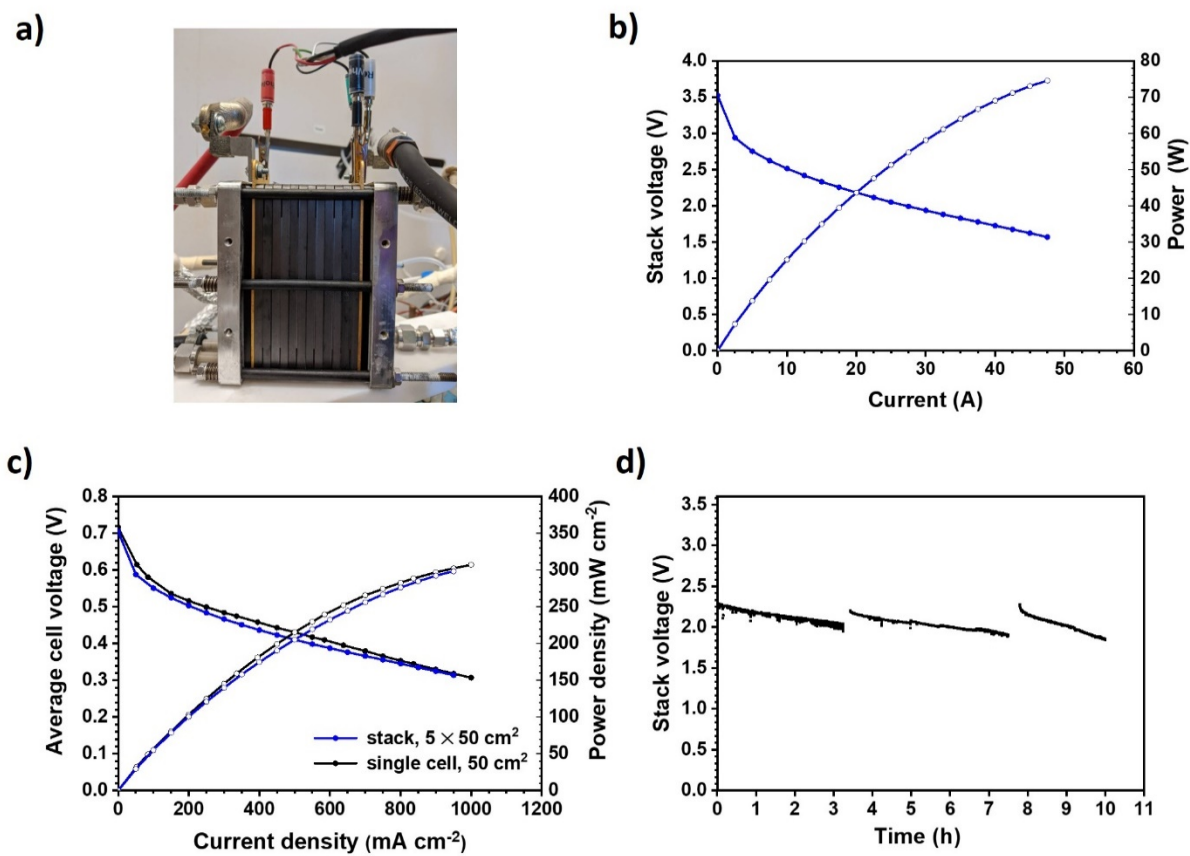


Fig. 5 | Image, performance, and durability of 5-cell stack. **a**, Illustration of 5-cell DAFC stack. **b**, Polarization and power density curves of DAFC. **c**, The comparison of polarization and power density curves of DAFC stack and a 50 cm^2 single cell. Test conditions: cell temperature of $90 \text{ }^\circ\text{C}$, cathode humidifier temperature of $90 \text{ }^\circ\text{C}$, 25 mL min^{-1} 7 M NH_3 in 3 M KOH at 2 bar_g , 0.5 L min^{-1} O_2 with a humidifier at $95 \text{ }^\circ\text{C}$ and 3 bar_g . **d**, short-term stack stability test at 15 A operating at $90 \text{ }^\circ\text{C}$. Anode: $2 \text{ mg}_{\text{PGM}} \text{ cm}^{-2}$ PtIr/C with PiperION PAP-TP-100 ionomer. HEM: PiperION membrane ($13 \text{ } \mu\text{m}$ thickness, reinforced PAP-TP-85). Cathode: 1.2 mg cm^{-2} Co_2MnO_4 with $20 \text{ wt}\%$ PiperION PAP-TP-100 ionomer.

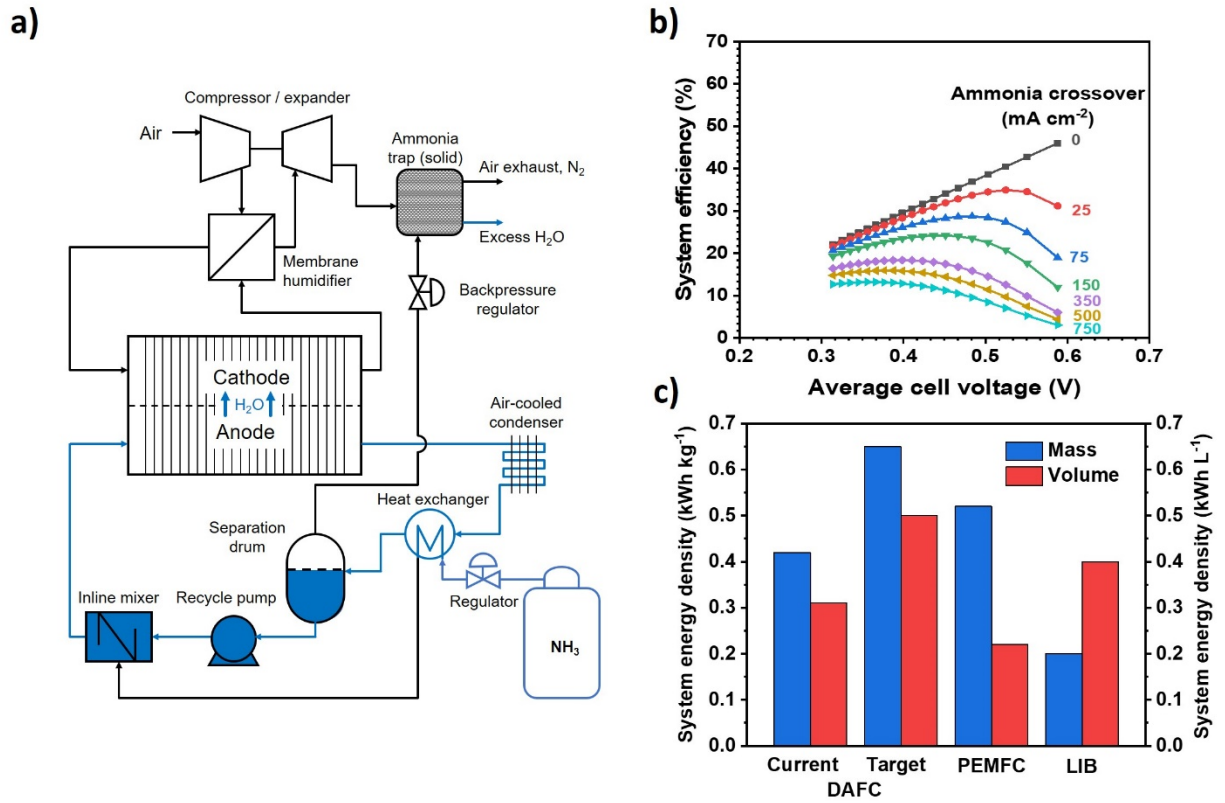


Fig. 6 | Proposed 2 kW, 10 kWh DAFC-based system. a, The proposed process flow diagram of 2kW DAFC-based system. **b,** System efficiency as a function of ammonia crossover. **c,** Energy densities of DAFC, PEMFC, and Li Battery-based systems, respectively.